Application of the cross-disperser method joint with the two-phonon acousto-optical interaction to optical spectrum analysis

Technical Report No. 643

Principal contributors:

Alexandre S. Shcherbakov, Adán Omar Arellanes, and Vahram Chavushyan.

National Institute for Astrophysics, Optics, and Electronics (INAOE), Puebla, Mexico.

National Institute for Astrophysics, Optics, and Electronics (INAOE),

Puebla, Mexico.

Department for Optics, INAOE

Index

ABSTRACT.

We develop an advanced approach to the optical spectrometer with acousto-optical dynamic grating for the Guillermo Haro astrophysical observatory (Mexico). The progress consists in two principal novelties. First one is using the acousto-optical nonlinearity of two-phonon light scattering in crystals with linear acoustic losses. This advanced regime of light scattering exhibits recently revealed additional degree of freedom, which allows tuning the frequency of elastic waves and admits the nonlinear apodization improving the dynamic range. The second novelty is combining the cross-disperser with acousto-optical processing. Similar pioneer step gives us an opportunity to operate over all the visible range in parallel regime with maximal achievable resolution. The observation window of optical spectrometer in that observatory is ~9 cm, so that the theoretical estimations of maximal performances for a low-loss $LiNbO_3$-crystal for this optical aperture at $\lambda = 405$ nm give the spectral resolution 0.0523 Å, resolving power 77,400, and number of spots 57,500. The illustrative proof-of-principle experiments with 6-cm $LiNbO_3$-crystal have been performed.

1. INTRODUCTION

The acousto-optical (AO) spectrometers have their roots in the end of 1960s with the creation of the collinear AO filters by Harris & Wallace [1], where optical and acoustical wave were collinear. In these devices, a polarized light beam is incident in the AO cell made of an anisotropic crystal. A piezoelectric transducer attached to the cell produces the acoustic wave. After that, the crossed polarizers are used to analyze the signal. This process implies a need to scan over the range of interest to obtain the light spectrum sequentially by adjusting the frequency on the piezoelectric transducer. Later, the non-collinear AO filters appeared using the AO interaction when the directions of acoustic and light wave are not parallel to one another [2]. In these devices, the polarization of light is again shifted and analyzed with a polarizer. In this case, the process of filtering is going in parallel regime over the range of analysis, i.e. analyzing several wavelengths at the same time. There is also the opportunity to use the non-collinear AO interaction in anisotropic media to perform the filtering process. This case of analysis is very close to exploiting AO deflector, which is used as a dispersive component; and the setup for these spectrometers is very similar to a dynamic diffraction grating.

One potential advantage for the AO spectrometers is the possibility of ~ 100% efficiency in the AO interaction, which can be achieved by choosing the correct acoustic power density depending on the material parameters such as the AO figure of merit M_2 and the length of interaction [2,3]. The normal practice is to work with the first order of the AO interaction. Nevertheless, several studies had been made using the second and third orders [4,5]. Since 1970s, AO techniques had been used in astronomy to fulfill spectroscopic observations in ground-based telescopes and also within space-borne missions [6,7]. In previous investigations we have suggested the use of an AO cell as a dispersive component in the Guillermo Haro astrophysical observatory spectrometer [8]. To improve the resolution of that device one had to grow larger crystals for the cell, which is very difficult and expensive. In this work, we are proposing the exploitation of the two-phonon AO interaction, which can be used with the same cell size and also can double the spectral resolution.

Nevertheless, within the last years the studies of a breakthrough novelty related to the optical spectrum analysis of high resolution and efficiency had been carried out in nonlinear acousto-optics. They are related to both one-phonon collinear [9,10] and two-phonon non-collinear [11,12] AO interactions in various crystalline materials. These studies are concentrated around the AO nonlinearity governed by elastic waves of finite amplitude in effective crystals with significant acoustic attenuation. As a result, the best to our knowledge spectral resolution $\delta\lambda$ and resolving power R had been found theoretically and then experimentally.

Now, we present subsequent development of those studies related to precise parallel optical spectrum analysis based on low-loss AO materials. After comparison analysis of a few crystals, we have chosen an advanced wide-aperture non-collinear lithium niobate (LiNbO$_3$)-crystalline AO cell providing as better as possible to-day spectral resolution and desirable nonlinear apodization. That analysis is confirmed by the proof-of-principal experiment for the key point of our new investigations. Additionally, now we propose to

joint the recently obtained findings in nonlinear acousto-optics with the cross-disperser technique [13] to obtain an opportunity for the parallel optical spectrum analysis of high resolution in a wide spectral range. In fact, we have carried out, as far as we know, the first observation of a two-phonon light scattering in $LiNbO_3$-crystal, which had been implicitly predicted previously [14].

In section 2, the two-phonon light scattering is introduced with the needed references and, after frequency characterization, $LiNbO_3$ crystal is chosen as the most acceptable for further analysis. In section 3, optical surfaces for the two-phonon light scattering in $LiNbO_3$-crystal are considered to note the importance inherent in the revealed degree of freedom. The cross-disperser technique, needed for the parallel optical spectrum analysis of high resolution in a wide spectral range, is considered in Section 4 to estimate performances of the AO cell. Section 5 describes the pre-experimental estimations needed for the use of $LiNbO_3$ crystal in the two-phonon AO cell. In Section 6, we represent the results of our proof-of-principle experiments. Briefly explained conclusive remarks are placed in Section 7.

2. FREQUENCY CHARACTERIZATION FOR LOW-LOSS UNIAXIAL CRYSTALS

Strongly nonlinear behavior of optical components within the Bragg AO interaction in anisotropic medium can be achieved in usual experiment without any observable influence of the scattering process on the acoustic wave [3,4]. Let us assume that the area of propagation for the acoustic wave, traveling almost perpendicularly to the light beams, is bounded by two planes $x = 0$ and $x = L$ in a uniaxial crystal and take into account both angular and frequency mismatches in the wave vectors. Usually, the Bragg AO processes include three waves: incident and scattered light modes as well as an acoustic mode [3,4], and incorporate conserving both the energy and the momentum for each partial act of a one-phonon scattering. However, under certain conditions, i.e. at a set of the angles of light incidence on selected crystal cuts and at fixed frequency of acoustic wave, one can observe Bragg light scattering caused by participating two phonons and the conservation laws are given by $\nu_1 = \nu_0 + f_2$, $\vec{k}_1 = \vec{k}_0 + \vec{K}$, $\nu_2 = \nu_0 + 2 f_2$, and $\vec{k}_2 = \vec{k}_0 + 2\vec{K}$, simultaneously (where ν_m, $\vec{k}_m$ and f_2, $\vec{K}$ are the frequencies and wave vectors of light and acoustic waves, $m = 0, 1, 2$). Such a four-wave process occurs at the frequency f_2 of acoustic wave, peculiar to just a two-phonon scattering, which can be determined as $f_2 = V b / \lambda$, where $b = |n_O^2 - n_E^2|^{1/2}$ is a dispersive birefringence factor and $n_O \neq n_E$ are the current refractive indices of a uniaxial crystal, V is the ultrasound velocity, λ is the incident light wavelength. The polarization of light in the zero and second orders is orthogonal to the polarization in the first order, whereas the frequencies of light beams in the first and second orders are shifted by f_2 and $2f_2$, respectively, with reference to the zero order.

Broadly speaking, there is very limited number of materials available for designing modern wide-aperture AO devices. This fact is conditioned by a large amount of various: optical, acoustical, and AO parameters, which should be accurately and reliably measured within wide optical and acoustical spectra. The results of similar measurements, performed during last 40 years, have been concentrated in bibliography in such a way that now one can restrict his attention within a few fundamental publications. The best and most useful of them, in our opinion, are Ref. [**15-17**] that had been used within this article to find and characterize the materials acceptable for our studies.

The analysis of these references shows that at the moment, only three low-loss crystals, providing the slow-shear elastic modes exploitation, can be considered for realizing a two-phonon Bragg light scattering due to their more or less acceptable physical characteristics. These crystalline materials manifest a reasonable level of total acoustic losses, relatively low velocities of acoustic waves, and give chance for a high enough efficiency for anomalous light scattering, which is in need for a two-phonon AO interaction. Let's characterize them sequentially.

2.1. Rutile TiO$_2$: S[001][110].

In 2008, a rutile-crystal based Bragg AO cell with 3 GHz bandwidth had been reported in connection with the development of ultra-wide band radio-wave AO spectrometer for radio-astronomy applications [18]. This cell had been designed for operation at $\lambda = 488$ nm, and its response had been centered at ~ 5 GHz with the flatness better than ~ 3 dB. The

geometry of that AO cell had chosen to perform so-called "tangential phase matching" one-phonon AO interaction.

Let us consider an opportunity to exploit almost this geometry of AO interaction for realizing a two-phonon light scattering. Broadly speaking, due to its spectral range is $\Delta\lambda \approx$ 0.45-6.0 μm, the main refractive indices of a TiO_2-crystal are about $N_O \approx 2.853$ and $N_E \approx$ 3.216 at $\lambda \approx 435.8$ nm, one can expect the maximal central frequency for a 2-phonon light scattering [4] close to $f_{2,max} \approx V \lambda^{-1} |N_E^2-N_O^2|^{1/2} \approx 10$ GHz, so that $f_2 \approx 5$ GHz is physically acceptable. For the acoustic frequency $f_2 \approx 5$ GHz with $\Gamma = 0.444$ dB/(cm GHz^2), linear acoustic losses exceed 11 dB/cm that practically excludes the optical aperture larger than D = 1 cm. Reasoning from $V = 3.3 \times 10^5$ cm/s for the slow-shear mode S[001][110] in rutile, one can estimate that the expected frequency resolution of AO cell in conventional scheme for spectrum analyzer [14] will be $\delta f = V/(2D) \approx 0.165 \times 10^6$ MHz, so that the ideal expected spectral resolution will be about $\delta\lambda \approx 0.161$ Å at $\lambda = 488$ nm mentioned above. These theoretical data for the spectral resolution cannot be considered directly in the presence of high acoustic losses about of 11 dB per aperture for AO cell, because the effect of nonlinear apodization [12] must be additionally taken into account. For such a level of acoustic losses, the resolvable spot size will be practically doubled. Therefore one can expect even theoretical spectrum resolution for blue light range close to $\delta\lambda \approx 0.3$ Å, which cannot be considered today as an attractive value as more as a lot of additional affecting factors have to be expected in practice.

2.2. Lithium tantalate LiTaO₃: S[100][010].

At the first glance, very low level of acoustic attenuation together with not very high velocity of acoustic waves can promises rather high spectral resolution with using lithium tantalate ($LiTaO_3$) as a material for Bragg AO cell. However, one has to take into account that this crystal has very small birefringence. This value is varied from one reference to another, but its maximal magnitude does not exceed $|N_O - N_E| \leq 0.005$ with $N_E \approx N_O \approx 2.2$ at $\lambda = 633$ nm [2]. By this it means that the maximal central frequency for a 2-phonon light scattering is limited by about $f_{2,max} \approx V \lambda^{-1} |N_E^2-N_O^2|^{1/2} \leq 100$ MHz. Consequently, with any reasonable $D \leq 9$ cm one arrives at the spectral resolution $\delta\lambda \geq 1$ Å, which is too far from the highest resolution achieved recently.

2.3. Lithium niobate LiNbO₃: S[100] 35° Y.

Let us require that the total losses per the optical aperture D = 9 cm should be not more than B = 6 dB/ap. For slow-shear mode S[100] 35° Y in $LiNbO_3$-crystal with $V = 3.6 \times 10^5$ cm/s and $\Gamma \approx 0.28$ dB/(cm GHz^2), such a requirement leads to the acoustic frequency $f_2 = [B/(D \Gamma)]^{1/2} \approx 1.54$ GHz. Then, this crystal has quite moderate birefringence, for example, $N_O \approx 2.4317$, $N_E \approx 2.3257$ at $\lambda = 405$ nm [2]. By this it means that the maximal central frequency for a 2-phonon light scattering is limited by about $f_{2,max} \approx V \lambda^{-1} |N_E^2-N_O^2|^{1/2} \leq 6.3$ GHz. After that, one can estimate the expected resolution within the two-phonon light scattering. Namely, the frequency resolution is $\delta f_T = V/2D \approx 20.0$ kHz at the light intensity level of 0.405 (the Rayleigh criterion), so that the expected theoretical spectral resolution is $\delta\lambda_T = \delta f_T \lambda/f_2 \approx 0.08165$ Å at $\lambda = 633$ nm and $\delta\lambda_T \approx 0.05226$ Å at $\lambda = 405$ nm, unfortunately, this crystal exhibits strong photorefraction in blue and ultraviolet range.

Nevertheless, LiNbO$_3$ crystal has the opportunity to shift the optical absorption edge to the ultraviolet light by being doped with Mg [10]. The previous would enable the use of such crystal for 370 nm optical wavelength and also that doping would reduce the optical absorption by almost four times. The presence of a dopant leads to the possibility of exploiting LiNbO3-crystal at even λ = 370 nm under action of not very intensive optical beams like starlight.

These estimations are looking definitely attractive in spite of possible influence of worsening practical factors. Thus one can make a deduction that the LiNbO$_3$-crystal can be considered as the best choice for resolving the above-formulated task.

3. OPTICAL SURFACES FOR THE TWO – PHONON LIGHT SCATTERING IN LINBO₃

The main refractive indices N_O and N_E in LiNbO₃.give $f_2 \approx 3.5$ GHz at $\lambda = 633$ nm and even $f_2 \approx 6.3$ GHz at $\lambda = 405$ nm. Such frequencies lead to extremely high acoustic losses, and to realize a two-phonon light scattering at a lower acoustic frequency, one has to consider involving recently found additional optical degree of freedom. It is based on exploiting the tilt angle within the geometry of two-phonon AO process at the chosen optical wavelength. LiNbO₃ is a uniaxial crystal, so that $n_O \equiv N_O$ is the main refractive index for the ordinary polarization, while n_E depends on the direction in the crystal. As before [11] one can consider the angle $\phi \in [0, \pi/2]$ of a tilt from the [001]-axis of a crystal. After the needed geometric consideration, one yields

$$\tan\phi = \lambda \, f_2 \, N_E / [N_O \sqrt{V^2(N_O^2 - N_E^2) - \lambda^2 f_2^2}\,]. \tag{1}$$

At this step, to make more concrete our consideration the LiNbO₃-crystal as an appropriate AO material will be analyzed. The elastic mode S[100] 35° Y in LiNbO₃ allows a two-phonon light scattering and can be considered as desirable alternative operating at rather different acoustic frequencies. The process of non-collinear two-phonon light scattering is represented in Fig. 1 in terms of two surfaces for the refractive indices of ordinary (see an external bright sphere) and extraordinary (see an internal dark ellipsoid) light waves for a trigonal crystal at the fixed optical wavelength λ. Generally, the sizes of both these surfaces are varied depending on λ due to a remarkable dispersion of the crystal within potential optical range.
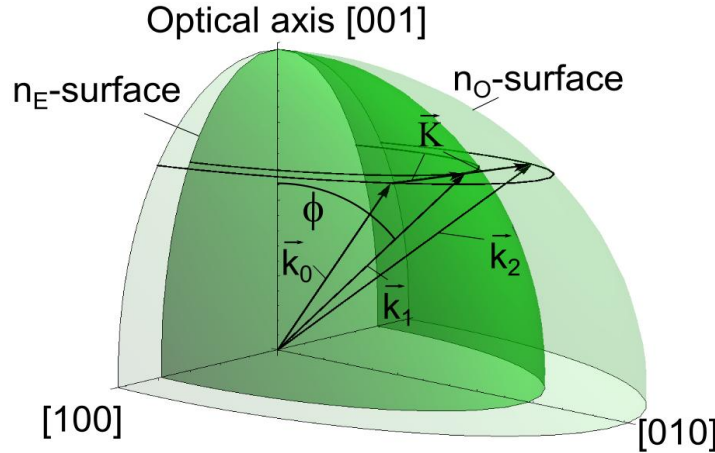
Fig. 1. Vector diagrams of two-phonon light scattering with the fixed ratio V/λ in LiNbO₃ crystal. The extraordinary refractive index n_E is described by an internal dark ellipsoid, while an external bright sphere shows the ordinary refractive index $n_O \equiv N_O$; the tilt angle ϕ, counted from the optical axis, is depicted.

The vertical axis in Fig. 1 is oriented along the optical [001]- axis of a crystal, while orientation for a pair of the horizontal axes depends on the chosen elastic mode (the scales of the wave-vector surfaces are not conserved for clearer representation). For LiNbO₃ crystal, in particular, they can be taken as [100] and [010] axes for the slow-shear acoustic mode. Then, this figure represents the vector diagram, illustrating an opportunity for the

two-phonon light scattering through various angles; which includes an optimal acoustic frequency with the birefringence factor b adequate to the chosen λ. A triplet of vectors, going from the geometric center of the surfaces, represents the optical wave vectors describing the corresponding orders of light scattering, whereas a pair of the sequential acoustic wave vectors $\bar{K}$ reflects the two-phonon process. The tilt angle ϕ characterizes an angle between the optical axis and the plane of scattering.

The availability of the angle ϕ signifies the existence of an additional physical degree of freedom inherent in the nonlinearity of the two-phonon light scattering. This degree of freedom permits the fixed frequency f_2 to exert control over various optical wavelengths scattered through different angles. In this case, one has to consider two pairs of surfaces peculiar to the refractive indices of ordinary and extraordinary light waves for a trigonal crystal in crystallographic plane and each similar pair of surfaces will correspond to an individual light wavelength. Taking the value B = 6 dB/aperture, one can find the central frequency for a two-phonon light scattering as $f_2 = [B/(\Gamma D)]^{1/2} = 1.54$ GHz.

4. SYNTHESIS OF A TWO-STEP SPECTRUM ANALYSIS

At this stage, we are doing a principally important step directed to the progress of AO spectrum analysis for optical signals. The main goal of this step is the synthesis of recently obtained findings related to the AO nonlinearity within non-collinear two-phonon light scattering by elastic waves of finite amplitude in crystals with the cross disperser technique [13].

For this purpose, two spectrometers will be combined sequentially. First, the prism spectrometer will spread the incident optical wave using two dispersion prisms. The first prism is used to disperse the light and the second prism is used to collimate it, see Fig. 2a. As a result, the initial light beam will be expanded and the components of the incident light spectrum will be separated in optical wavelengths, parallel to each other. In figure 2b, the wave vector diagram is depicted in the plane of scattering. It shows that polarization for incident and scattered light lie in this plane. The eigen states for light polarization are described in Section 5. Then, these portions of the spectrum will be manipulated to form the needed tilt and Bragg angles to prepare them for the incidence on the AO cell, which represents the second spectrometer, see Fig 2c.
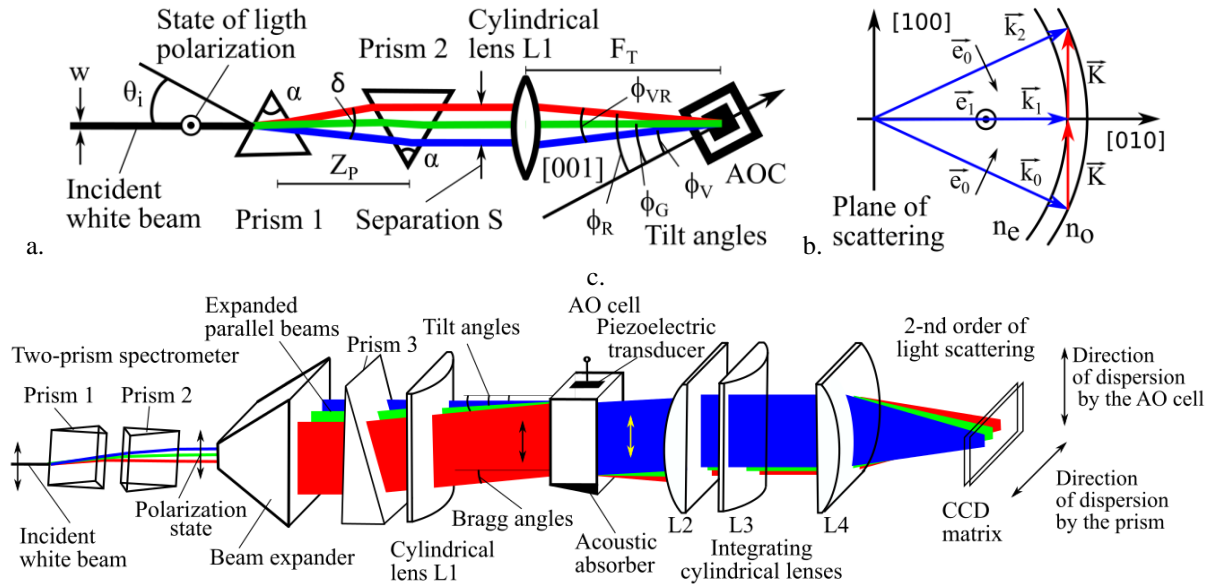
Fig. 2. Two-step AO spectrometer using the cross disperser; a) the upper view of the AO cell with the tilt angles, b) the wave vector diagram on the plane of scattering with the polarization of incident and scattered light , and c) the complete layout of the system, beam expander and prism 3 are not shown in a) for simplicity. S is the distance between the parallel optical beams and w is the size of the incident white beam.

The prism spectrometer has a low spectral resolution $\delta\lambda_P$, but a high spectral bandwidth $\Delta\lambda_P$. In contrast, the AO cell, working in the two-phonon regime, has a high spectral resolution $\delta\lambda_{AO}$, but very narrow spectral bandwidth $\Delta\lambda_{AO}$. To exploit really high resolution of the AO cell, a pair of spectrometers should proceed a combined analysis similar to the one used in cross-disperser spectrographs. This process spreads roughly the entire spectrum (with prisms as the dispersive component for a "coarse" resolution) and later each portion of the spectrum will be dispersed again (with the use of an AO cell with a high spectral resolution). The spectral resolution $\delta\lambda_P$ from the prism should coincide with the spectral

bandwidth $\Delta\lambda_{AO}$ of the AO cell, which is responsible for a high resolution that can be calculated as [19]

$$\delta\lambda_P = (\lambda / w)(\partial \lambda / \partial n), \qquad (2)$$

where λ is the optical wavelength, w is the width of the incident beam (see Fig. 2a), which should be equal to the effective base of a prism [19], and $\partial n/\partial\lambda$ is the chromatic dispersion of the prism refractive index. The prisms are intended to work within the visible range, which means a spectral range $\Delta\lambda_P \approx 300$ nm.

4.1. Tilt and Bragg Angles

The tilt angle for each optical wavelength must be created before the light enters the AO cell. The relation between tilt angle ϕ and optical wavelength λ is described by Eq.(1). After expanding the beam by the beam expander, a cylindrical lens is used to focus the beam on the AO cell. Together with this an individual tilt angle has to be made for each optical wavelength. In our case of 2-phonon AO interaction, the goal is to form the angle difference of $\phi_{VR} = \phi_R - \phi_V \approx 11.79°$, see data in Table 1, between the violet (sub-index V, $\lambda = 405$ nm) and the red (sub-index R, $\lambda = 633$ nm) optical wavelengths. Thus, the angle between the optical axis of the focusing lens and the optical axis of the AO cell must be ($\phi_R + \phi_V$) / 2 $\approx 19.445°$, this would be the tilt angle of the center optical wavelength ($\lambda \approx 520$ nm) in the range. The focal distance of the focusing lens should be estimated to make the correct tilt angles on the AO cell. For example, if the expanded beam has the separation S = 2 cm (as depicted in Fig. 2a), the needed focal distance F_T (sub-index stands for the tilt angle) can be calculated using the trigonometric relation tan $\phi_{VR} = S/F_T$, so the focal distance should be equal to $F_T \approx 10$ cm.

In order to make the separation of the extreme wavelengths in the input light beam, a pair of prisms has to be taken. First, these prisms will deflect each optical wavelength in different angles and then, after a proper distance, the second prism will compensate those deflections and shape the entire spectrum in parallel beams. The material of the prisms must be selected carefully to avoid the potential non-uniform spreading of the optical spectrum due to the non-linear chromatic dispersion. For instance, dense flint glass (Schott N-SF11) has almost linear chromatic dispersion in the visible range and small reflectance for the P-polarized light [20].

For an individual wavelength λ, the deviation angle $\delta(\lambda)$ (measured from the incident angle θ_i) of the prism is [19]:

$$\delta = (\theta_i - \alpha) + \arcsin[\sin \alpha \sqrt{(n_p^2 - \sin^2 \theta_i)} - \sin \theta_i \cos\alpha], \qquad (3)$$

where θ_i is the angle of incidence in the prism, α is the characteristic angle of the prism, and $n_p(\lambda_c) \equiv n_{p,c}$ is the refractive index of the prism for that wavelength λ. Then, the angle between the extremes of the spectrum is $\delta_{VR} = \delta(\lambda_R)-\delta(\lambda_V)$.

Table 1. Two-phonon light scattering in LiNbO$_3$ crystal at 1.543 GHz with D = 9 cm and δf$_T$ = 20 kHz.

Wavelength λ, nm	n$_O$	n$_E$	Tilt angle φ, deg.	Bragg angle θ$_0$, deg.	Δf$_T$, MHz	Δλ$_T$, Å	δλ$_T$, Å	N$_T$
370	2.496	2.491	11.66	3.636	4.72	11.32	0.0479	236
405	2.432	2.426	13.55	4.083	4.20	11.03	0.0525	210
532	2.323	2.312	20.16	5.606	3.06	10.54	0.0690	152
633	2.287	2.270	25.34	6.767	2.52	10.37	0.0820	126

The larger angles α would allow higher deviation angles δ$_{VR}$. At the same time, these large angles α lead to higher reflection coefficients and even total internal reflection in the second facet of the prism. Nonetheless, small angles α can avoid total internal reflections, but the deviation angles δ$_{VR}$ in this case would be very small for any angle of incidence. We have taken two equilateral prisms (α = 60°), because they have large deflection angles and allow us relatively large stable zone with high deflection angles.

Due to this, the total length of the optical system could be minimized in comparison with the use of prisms with smaller deflection angles. The use of materials with relatively high refraction index and, what is more important, high chromatic dispersion produces relatively larger dispersion angles. Nevertheless, the deflection angles are small, i.e. close to δ ≈ 8° with an incident angle θi ≈ 61° (that is close to the Brewster's angle to have the best transmittance). As an example, let the maximum separation between the extreme parallel rays is S = 2 cm. The necessary distance Z$_p$ between the prisms (required to achieve a 2 cm separation), must follow the equation sin δ = S/Z$_p$, so we can estimate Z$_p$ ≈ 14 cm. The length Z$_p$ of the prism pair can be reduced by choosing remarkably smaller separation S between the blue and red optical wavelengths. The previous analysis imply selecting a collimating lens with smaller focal length F$_T$ = S / tan φ$_{VR}$, from Eq. (3). This also would require a smaller prism size, which will worsen the coarse resolution of the prism system. Also, the expanded beam must be declined to ensure that each optical wavelength will be directed at the correct Bragg angle when the AO cell is reached. Providing the correct Bragg angles for each wavelength is not very easy due to the cylindrical symmetry of the system. Each wide beam (with its corresponding wavelength) should be declined to coincide with the needed Bragg angle θ$_0$. All the previous considerations allow us to take these optical components to create the tilt and Bragg angles within the AO cell. Now, we need to extrapolate these results to make it possible the usage of a 9 cm AO cell, which is necessary to improve the spectral resolution of such a system.

4.2. The Cross Disperser Technique

A two-stage process for improving the resolution of spectrometers has been developed previously for prisms and echelle gratings (cross-dispersed). Such a process first disperses the light in one axis at the first stage. Then, in the second stage, the light is dispersed once again but now in a different direction. Next is the description of how our AO spectrometer uses a two-stage process with dispersive components to enhance the spectral bandwidth. Here, we are applying this technique using a dispersive prism and an AO cell, the first time to our knowledge that this combination of spectrometers is used. At the first stage, our spectrometer will use traditional prisms, which will disperse the optical wave with a low

resolution (coarse resolution). Then, in the second stage, the AO cell will disperse the light in a perpendicular direction and create a 3-D distribution of the spectrum intensity, see Fig. 3. Just this extra dimension is the responsible for the high resolution achieved by our AO spectrometer.

One illustrative spectrum will be used to show the potential capabilities of our AO spectrum analyzer and demonstrate how a high resolution can be achieved. The artificial spectrum used here has several peaks over the visible range.

Seven principal signals with very different spectrums have been considered. For example, let the group of five peaks near the zone of 500 nm to have 2 signals; one of them (A) has four peaks and the other one (B) has only one peak. The spectra of signals A and B are separated by about 2 nm along the axis $\Delta\lambda_P$, and this fact allows us to identify them like definitely different signals. These signal difference of 2 nm represent the limit of the spectral resolution of the prism spectrometer that can be recognized one from another. Nevertheless, four peaks of signal A include peaks in more than one wavelength, which are very close to each other (in their spectra) and would not be resolved with traditional prism spectrometer.

Such spectra are shown as one individual line if the plot in Fig. 3 is projected over the $\Delta\lambda_P$ axis. In contrast, the same spectrum can be fully resolved using the combination of prism and AO cell spectrometers. For instance, the separation of peaks of the first 3 signals (at the left of Fig. 3) is about 0.05 nm. The axes of the Fig. 3 show the prism spectral bandwidth $\Delta\lambda_P$ (from 400 nm to 700 nm), which has the resolution of a traditional prism spectrometer. The high resolution (with a spectral bandwidth $\Delta\lambda_{AO}$ of about 0.75 nm), i.e. the resolution achieved thanks to the AO cell, is shown on the other axis and just this resolving power enable us to separate and distinguish the signals with very close peaks in their spectrum.
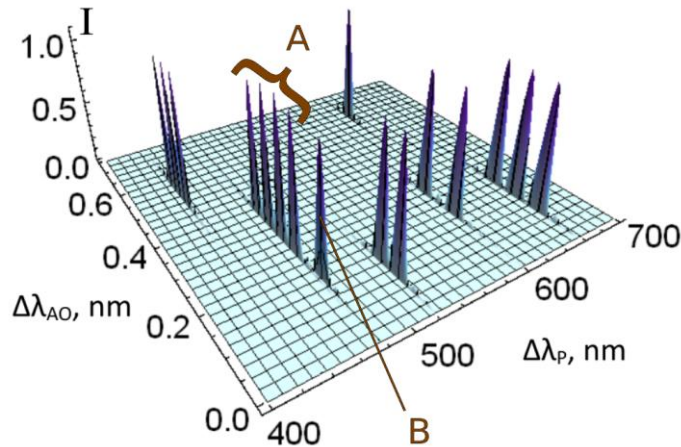
Fig. 3. Illustrative optical spectrum analyzed with a two-step AO spectrometer. The height of the peaks is the relative light intensity I. The rest of the axes are measured in nanometers.

The spectral bandwidth $\Delta\lambda_{AO}$ of the AO cell is calculated as:

$$\Delta\lambda_{AO} = (\lambda / f_2)\, \Delta f_2 \approx n_i V^2 /(2\, f_2^2\, L)\,. \tag{4}$$

14

where f_2 is the fixed acoustic frequency applied to the AO cell, Δf_2 is the frequency bandwidth of the AO cell (see Eq.(18a) in Ref. [11]) and L is the AO interaction length. As previously mentioned, this narrow spectral bandwidth should match with the "coarse resolution" of the prism spectrometer. Then, matching Eqs. (2) and (4) we can estimate **w** as:

$$w = (\lambda / \Delta\lambda_{AO})(\partial\lambda / \partial n). \tag{5}$$

Also, the resolution achieved by the 2-phonon AO cell is estimated by the equation $\delta\lambda_{AO} \approx \lambda V/(2 f_2 D)$ [11]. Following the previous example of an AO cell made of LiNbO$_3$, one can estimate the spectral bandwidth as $\Delta\lambda_{AO} \approx 11.03$ Å, see Eq. (4).

The tilt angles ϕ are different for each optical wavelength, so that the optical beam will be declined at the input of the AO cell. Then, its width should be small enough to not exceed the size of the acoustic beam column in the AO cell. For this purpose, we are considering a ratio between the length and the width of the acoustic beam as L : H $\approx$ 3:1. Considering the case of a prism with $\partial n/\partial\lambda \approx$ -0.63953 μm^{-1} (SCHOTT flint glass N-SF11), and the needed "coarse resolution" as $\delta\lambda_P \approx 11.03$ Å at $\lambda = 405$ nm, the required beam width would be w = 0.557 mm according to Eq. (5).

Thus one can formulate advanced performances due to the synthesis of a two-step spectrum analysis combining the prism spectrometer with the AO spectrometer as it has shown in Fig.2. The developed estimations show that the contribution of prism spectrometer consists in shaping the number M of resolvable spots together with enabling the parallel spectrum analysis within all the spectrum range available for prism's material. In fact, a pair of prisms will spread the incident (white) light beam of the spectrum width $\Delta\lambda_P$ into M portions of a spectrum with a low spectral resolution, so that each portion will have the size $\delta\lambda_P$. This number is given by M = $\Delta\lambda_P/\delta\lambda_P$ = (w/λ) (λ_R - λ_V) ($\partial n/\partial\lambda$).

Then, the AO cell will take each of these portions of the spectrum and stretch them to see with a high resolution and limited number of resolvable spots N. Finally, the total spectrum will be converted into a 2D-distribution, see Fig.3, which represents the synthesis of N rows and M columns, i.e. has a dimension of (N $\times$ M) resolvable wavelengths of the spectrum under analysis. In our case, this would enable us to characterize N = 236 from Table 1 and M = 244, for example at $\lambda = 405$ nm, so that the product N $\times$ M = 57,584 resolvable spots in the visible range simultaneously and achieve a resolving power R $\approx$ 77,140. With these estimations of resolvable spots, one can formulate the requirements to the CCD as a matrix with a minimum of 472 $\times$ 488 pixels in agreement with the sampling theorem [21]. These estimations will be significantly changed at $\lambda = 633$ nm, so that one will have N $\times$ M = 126 $\times$ 156 = 19,600 spots. However, an acceptable number of pixels within the CCD photo-detector can be taken the same as more as a spot's size at this light wavelength will be even larger.

5. PRE - ESTIMATIONS OF THE LINBO₃-MADE AO CELL

At the moment, we have unfortunately only a lithium niobate crystalline sample of the needed orientation and high optical quality with D = 6.0 cm for carrying out experiments. This is why, using the above-obtained maximal estimations, now we are forced to re-estimate potential performances for the LiNbO₃ made AO cell with the reduced aperture. Moreover, the available sample is not doped by Mg that usually improves performances of similar AO cell within a blue part of spectrum. We have analyzed this problem in detail previously [10] in connection with astrophysical applications and found the corresponding limitations. Currently, we consider those limitations as perfectly applicable for potential exploitation of the cell under discussion here. Generally, the usage of LiNbO₃ with no dopant will result in partially smaller spectral bandwidth of operation compared with the 4% Mg doped LiNbO₃. Also, it would imply a larger value of optical absorption, which reduces the efficiency of AO cell. However, both these demerits can be simply re-calculated for the doped crystal. Additionally, one can note that the effect of photorefraction under action of star light had been estimated previously for exactly collinear geometry of AO interaction with the small optical aperture of about $\sim 2 \times 2$ mm². While now we consider the aperture 60×2 mm², which provides much smaller optical power density from the same star-like sources of light.

To make current pre-experimental estimations as close as possible to the above-performed analysis we will keep the total level of linear acoustic losses at the same level B = 6.0 dB/aperture due to choosing the higher central acoustic frequency $f_2 \approx 1.9$ GHz. Then, because of the possibility obtained from the cross-disperser technology, one can take the sizes of piezoelectric transducer equal to $L \times H = 0.6 \times 0.2$ cm². It is easy to find that these values lead to satisfying with a margin the well-know inequality for Klein-Cook parameter $Q = 2\pi \lambda L f_2^2/(n_0 V^2) \gg 1$, which provides the Bragg regime for AO interaction when $L \approx$ 0.6 cm. Together with this, lying an acoustic beam within the Fresnel acoustic zone is guaranteed as well that makes possible to omit potential angular divergence of acoustic beam.

Then, let us estimate the efficiency of the two-phonon light scattering in low-loss LiNbO₃ crystal. To obtain the AO figure of merit M_2 the effective photo-elastic constant p_{eff} has to be found. In so doing, one has to write the deformation tensor $\gamma = (\vec{u} \cdot \vec{q} + \vec{q} \cdot \vec{u})/2$, where $\vec{q} = \vec{K}/|K|$ and $\vec{u}$ is the unit displacement vector. We work with the trigonal LiNbO₃-crystal (symmetry group 3m) and consider the case of the slow-shear elastic mode with S[100] 35° Y, see Fig. 2b. In this case $\vec{q} = (1, 0, 0)$ and $\vec{u} = (0, \cos \psi, \sin \psi)$ with $\psi = \angle (\vec{u}, [010]) = 35°$. The deformation tensor γ in the form of a 3×3 matrix with the components γ_{kl} (k, l = 1, 2, 3) can be converted into a 6-dimension vector $\gamma = (0, 0, 0, 0, \sin \psi, \cos \psi)$, while the photo-elastic tensor p should be converted into the form of a 6×6 matrix with the components $p_{\lambda\mu}$. Now, we can find the matrix product $\hat{p}\hat{\gamma} = (u_2 p_{41} + u_3 p_{44})(\vec{e}_3 \cdot \vec{e}_1 + \vec{e}_1 \cdot \vec{e}_3) + (u_2 p_{66} + u_3 p_{14}) (\vec{e}_2 \cdot \vec{e}_1 + \vec{e}_1 \cdot \vec{e}_2)$ in dyadic notations and then convert it back to the form of a standard tensor $(p\gamma)$. After that, the effective photo-elastic constant can be written as $p_{eff} = \vec{e}_1 (p\gamma)\vec{e}_0$, where the unit vectors $\vec{e}_0$ and $\vec{e}_1$ describe the eigen states of polarization for incident and scattered light beams, respectively. Within the

16

anomalous light scattering (specific for a two-phonon AO interaction), the eigen polarization vectors $\vec{e}_0$ and $\vec{e}_1$ should be orthogonal to one another $\vec{e}_0 \perp \vec{e}_1$ and to the light beam wave vector $\vec{k} = (0, \sin\phi, \cos\phi)$, where $\phi = \angle(\vec{k}, [001])$. However, they both $\vec{e}_0$ and $\vec{e}_1$ should be lying in a plane, determined by the mutually orthogonal unit vectors $\vec{\zeta}_1 = (1, 0, 0)$ and $\vec{\zeta}_2 = (0, -\cos\phi, \sin\phi)$, including the vector $\vec{K} \| [100]$. Thus, one can take $\vec{e}_0 = (\cos\gamma, -\cos\phi\sin\gamma, \sin\phi\sin\gamma)$ and $\vec{e}_1 = (-\sin\gamma, -\cos\phi\cos\gamma, \sin\phi\cos\gamma)$, where $\gamma = \angle(\vec{e}_0, [100])$ and $\vec{e}_0 \cdot \vec{e}_1 \equiv 0$. As a result: $p_{eff} = 0.5\cos(2\gamma) \times [(p_{44}\sin\psi + p_{41}\cos\psi)\sin\phi - (p_{66}\cos\psi + p_{14}\sin\psi)\cos\phi]$.

To provide existing the optical eigen vectors one has to take either $\gamma \approx 0$ or $\gamma \approx \pi/2$. However, both these opportunities give $\cos(2\gamma) = 1$, and p_{eff} will depend on two angles $\psi = 35°$ and ϕ. Now, p_{eff} can be computed with $p_{14} = -0.075$, $p_{41} = -0.151$, $p_{44} = 0.146$, and $p_{66} = -0.053$ [2]. The maximum value is $p_{eff, max} \approx 0.048$. With $\rho = 4.64$ g/cm^3, $n_O \equiv N_O = 2.432$ and $n_E \approx 2.426$ at $\lambda = 405$ nm, one yields $M_2 = n_O^3 n_E^3 (p_{eff, max})^2/(\rho V^3) \approx 2.186 \times 10^{-18}$ s^3/g.

After that, one has to estimate the effect of the nonlinear apodization appearing due to combined action of the AO nonlinearity and linear acoustic losses in LiNbO3-crystal in the vicinity of the first maximum. For this purpose, we can apply the analysis developed in section 3 of Ref.[12], where the case with B ≈ 6 dB/aperture in particular had been analyzed exactly for the first maximum. Using the notation from that section, one can write at once the amplitude factor of linear acoustic losses $\alpha = 0.1152 \Gamma f_2^2 \approx 0.115$ cm^{-1}, the dimensionless profile parameter $\beta \approx 1.105$, the correction factor $\kappa \approx 1.04$ for a resolvable spot size due to apodization, and explain the optimized acoustic power parameter $\sigma_{1,Opt} \approx 1.1 \sigma_1$ cm^{-1} after the procedure of symmetrization.

Now, we are ready to perform important numerical estimations inherent in the non-collinear interaction at $\lambda = 405$ nm in the LiNbO$_3$ crystalline cell with $M_2 \approx 2.186 \times 10^{-18}$ s^3/g and L = 0.6 cm. The periodicity of the unit-level AO interaction maxima gives us an opportunity to choose the first maximum with lowest acoustic power density at $(\sigma x)_1 \approx 2.22$. Now, putting $x \equiv L$, one can find $\sigma_1 \approx 3.7$ cm^{-1}. The standard definition for σ [9], with $\cos\theta \approx 1$, leads to:

$$P_1 \approx 2\lambda^2 \sigma_1^2/(\pi^2 M_2) \ . \tag{6}$$

Consequently, Eq.(6) gives $P_1 \approx 208$ W/cm^2 = 2.08 W/mm^2, while after optimization $P_{1,Opt} \approx 2.517$ W/mm^2 for the first maximum with $\sigma_{1,Opt} \approx 4.07$ cm^{-1} at $\lambda = 405$ nm.

For the LiNbO$_3$-made AO cell with D = 6 cm and L ≈ 0.6 cm, the obtained pre-experimental theoretical estimations are summarized in Table 2. These estimations are related only to the first (i.e. with m = 1) of recently found maxima [11] in a distribution of light scattered into the second order due to non-collinear two-phonon AO interaction. One can see from this table that rather high spectral resolution can be achieved in LiNbO$_3$-made AO cell with the exploitation of the slow-shear elastic mode S[100] 35°Y. Consequently, these data show that further development of a new approach to optical spectrum analysis is

definitely desirable due to its improved spectral resolution. In acousto-optics, the spectral and frequency resolutions as well as the frequency and spectral bandwidths are connected with one another by the following theoretical relations $\delta\lambda_T = \delta f_T \, \lambda/f_2$; $\Delta\lambda_T = \Delta f_T \, \lambda / f_2$, respectively, where $\delta f_T = V/(2\,D)$ and $\Delta f_T \approx n_0 \, V^2/(2\,\lambda\,L\,f_2)$ for the first maximum. Then, one can find the theoretical number of resolvable spots as $N_T = \Delta f_T / \delta f_T = \Delta\lambda_T / \delta\lambda_T$.

6. PROOF-OF-PRINCIPAL EXPERIMENTAL DATA

6.1. Experiment Arrangement

Our proof-of-principal experiments were performed with the specially designed wide-aperture Bragg AO cell based on the unique $LiNbO_3$ single crystal, which had an active optical aperture of about 60×2 mm^2, see Fig. 4. This pioneer AO cell was able to operate over all the visible and near ultraviolet range. Practically, we used optical wavelengths λ = 405, 532, and 633 nm, which combine the convenience of operating in the visible range with violet, green, and red lights, from the single frequency solid-state lasers CL-405-050-S, CL-532-050-S, and DL-633-050-S (CrystaLaser) with the best expected optical performances inherent in this cell. In fact, we used once again the optical scheme of the experiments presented in Ref. 12, Fig. 11 with some modifications, where only the 2-nd order of a two-phonon AO interaction was shown, for each individual light wavelength. The sources of light beams had about 50 mW output CW optical power with additional optical attenuators.

These attenuators served us to minimize optical power down to a star level (like, for instance, from Vega) of light radiation [10] and to suppress significantly the effect of photorefraction in $LiNbO_3$. The CW-light radiation had linear state of the incident light polarization oriented almost along the crystallographic axis [100] of that AO cell. The optical part of our experiments included a 15-mm Glan-Taylor linear polarizer (the extinction ratio ~10^5, Thorlabs) and a four-prism (Edmund Optics) beam expander. They dealt with the coherent light beams polarized in the plane of expanding and provided rather flat (non-uniformities were better than ~ 10%) optical beam profiles. During the experiments with the beam shaper rather accurate angular adjusting of the incident light beams had been achieved. By this it means that both the correct Bragg angles of incidence and the needed tilt angles had been optimized. The 3-inch achromatic doublet lens (Edmund Optics) with the focal length of about 85 cm had been used as the integrating lens.

The $LiNbO_3$-based AO cell was prepared to be governed by the radio-wave signals whose best acoustic performances were expected at the central frequency $f_2 \approx 1.9$ GHz. A set of electronic equipment for both generating and registering the corresponding electric ultra-high-frequency (UHF) radio-wave signals had been exploited. Initially, the slowly (manually) tunable UHF-signal was applied to the electronic input port of the non-collinear AO cell through a wide-band UHF-amplifier HD20089 (1.0 – 2.0 GHz) and the corresponding impedance-matching electronic circuits. The design of this cell, operating in the regime of the non-collinear two-phonon AO interaction, is presented in detail in Fig. 4. We had exploited the ZnO film piezoelectric transducer oriented along the Y-axes with the coupling factor about of 0.31 and the acoustic impedance 16.4 g/(cm^2 s). Due to the frequency constant 1.44 GHz μm, this orientation gives the thicker film, more adequate to the expected high-level signals, and provides better acoustical matching with the chosen cut of $LiNbO_3$, whose acoustic impedance is 16.7 g/(cm^2 s). It generated the slow-shear mode acoustic beam with the cross section of about 12 mm^2 at the length L $\approx$ 0.6 cm of AO interaction.
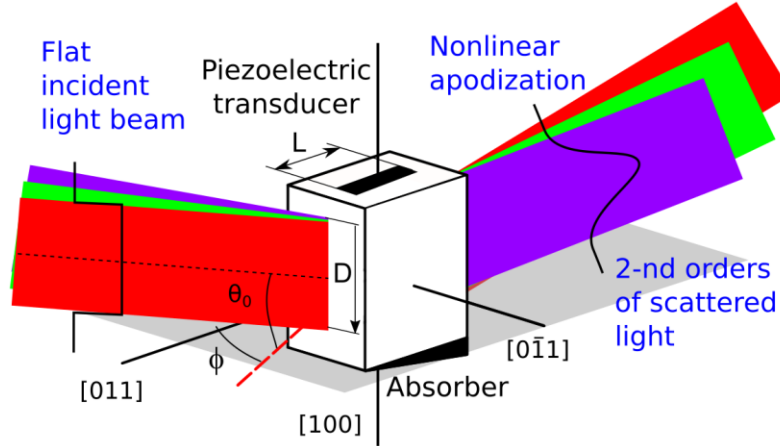
Fig. 4. Design of the LiNbO$_3$ made AO cell with L = 0.6 cm, H ≈ 0.2 cm.

Additionally, one has to take into account the losses needed for converting the electronic signal into an acoustic one, which are in practice close to $2 - 3$ dB. Usually, we have to restrict ourselves to a maximum level $P_{max} \leq 0.5$ W/mm^2 of acoustic power density. However, one can see from Table 2 that the above-found magnitudes for $P_{1, Opt}$ need applying the continuous-wave electric power at the levels close to $5 - 20$ W/mm^2, which exceeds significantly that P_{max}. This requires the absolute acoustic power < 110 W and the electric power < 220 W with the acoustic beam cross section of about 12 mm^2 in the AO cell under consideration. Similar levels of both electric and acoustic powers are definitely unacceptable for rather thin piezoelectric transducer at the central frequency $f_2 = 1.9$ GHz. To resolve this experimental difficulty we were forced to develop the needed pulse technique of operation to carry our trial illustrative experiments out.

Table 2. D = 6.0 cm with L ≈ 0.6 cm and beam width w = 0.557 mm. with δf$_T$ = 30 kHz, and f$_2$ = 1.9 GHz

| λ, nm	n$_0$	ñ$_E$	Tilt angle φ, deg.	Bragg angle θ$_0$, deg.	Δf$_T$, MHz	Δλ$_T$, Å	δλ$_T$, Å	N$_T$	κ d$_T$, μm	P$_{1, Opt}$, W/mm²	M$_2$ 10^{-18}, s³/g
405	2.432	2.422	16.70	4.997	3.43	7.35	0.0643	114	5.967	2.517	2.175
532	2.323	2.306	25.04	6.855	2.49	7.03	0.0845	83	7.612	5.807	1.636
633	2.287	2.262	31.74	8.270	2.06	6.91	0.1005	68	9.326	9.131	1.473

The goal of this pulse technique was the deterioration of loading the piezoelectric transducer by both electronic and acoustic signals to avoid any damages of thin enough resonant structure specific to that transducer. For this purpose, one was forced to use external signals with some pulse period-to-pulse duration ratio $\xi \geq 10$ in such a way that the average level of power density will be lower that the above-chosen value $P_{max} \approx 0.5$ W/mm^2. In so doing, the electronic part of that scheme should be added by the UHF modulator providing pulsed regime of operation with the required period-to-pulse duration ratios ξ. Then, the band-shapes of our AO cell at three optical wavelengths had been detected in the presence of AO nonlinearity. Our modified scheme therewith was under manual operation of tuning the acoustic carrier frequency from point to point in the vicinity of the central frequency $f_2 = 1.9$ GHz. In so doing, the observation of the band-shapes had been provided by a wide-aperture silicon photo-detector. By contrast, the resolvable spots had been measured exploiting a multi-pixel CCD array (SONY) consisting of 3.5 μm pixels with relatively long-time light energy collection.

6.2. Experimental Results

The experiments in pulsed regime of operation consisted of two parts. The first of them included detecting the frequency band-shape with a low oscillation damping, i.e. determining the effective bandwidth of the Bragg non-collinear two-phonon light scattering at a 0.405-maximum light intensity level. The detected band-shape had been observed within manual tuning of the UHF radio-wave carrier frequency from point to point with a regular frequency step ~100 kHz. Because of f_2 = 1.9 GHz, one can take the duration $\tau \approx$ 1.0 μs for the modulating rectangular pulse, which guarantied more than 1000 periods of the carrier frequency f_2 under envelope of this pulse. The photo-detection had been realized by a wide-aperture silicon photo-diode PDA36A (Thorlabs) in practically quasi-static regime due to detecting the count sequences by an oscilloscope. The accuracy of similar detecting was about 3-4%, which was considered as good enough for the needed estimations of frequency profile. Figure 5 shows an example of the experimental plot for the frequency band-shape inherent in the $LiNbO_3$-made AO cell with the damped piezoelectric transducer at the central frequency about 1.9 GHz and λ = 405 nm in the pulsed regime with ξ (405) ≥ 12. The total experimental frequency bandwidth at a 0.405-maximum light intensity level has been estimated by $\Delta f_M \approx$ 3.52 MHz.

The second part of experiments was related to estimating possible spectral resolution via measurements of the light intensity distributions specific to individual resolvable spots in the focal plane of the integrating lens for the light deflected by our AO cell into the second order. Precise optical measurements had been performed again at λ = 405, 532, and 633 nm to obtain sufficiently reliable estimations for the frequency resolution provided by the $LiNbO_3$ AO cell together with the above-described optical system, including the CCD array. The performed measurements had been done in the regime of the so-called "hot cell", i.e. with an UHF-signal applied at the input port of the $LiNbO_3$–cell. Figure 6 depicts the light intensity profiles with the spot sizes of about 7.02 and 10.98 microns with the side lobe levels of about 6.0%, respectively, which includes affecting the light distribution in a spot by the acoustic losses of 6 dB/ aperture. The produced measurements showed that the main lobe of each partial optical beam gave the spot size lighting almost two or three pixels, respectively, of the CCD-row that provided rather acceptable resolution from viewpoint of the sampling theorem.
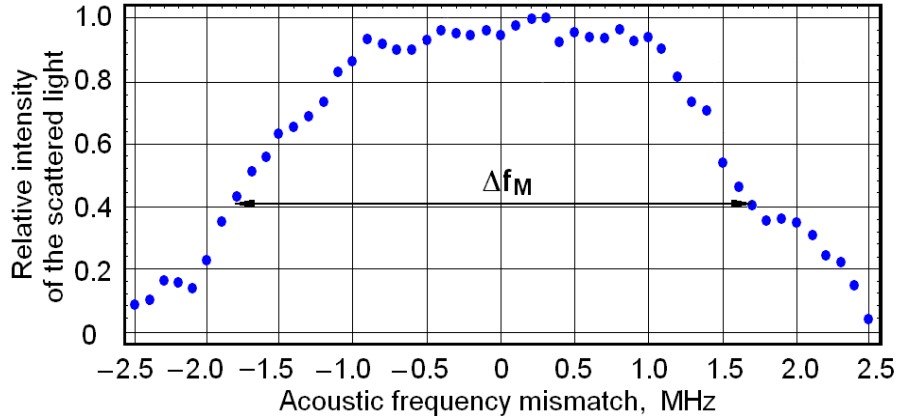
Fig. 5. Experimentally obtained frequency band-shape of the $LiNbO_3$-made AO cell at $f_2 \approx$ 1.9 GHz and λ = 405 nm.

As before, we used the integrating lens with $F = 85$ cm at $\lambda = 405$ nm, so that the theoretical spot sizes are $d_T = \lambda F / D \approx 5.737$ μm and $\kappa d_T \approx 5.967$ μm. Together with this, the plot in Fig. 6 exhibits the experimental spot size $d_M = \lambda F / D_M \approx 7.02$ μm that corresponds to the aberration factor $\zeta_M \approx 1.223$ (which includes various optical demerits of the system together with the correction factor $\kappa = 1.04$ of the nonlinear apodization) and to the effective aperture $D_M \approx 4.906$ cm for the AO cell. The last data show that about 18% of the active optical aperture of the AO cell is lost due to imperfectness of the lens and cell's crystalline material together with the effect of remarkable acoustic losses ∼ 6 dB/aperture. Therefore, instead of theoretical limit of the frequency resolution $\delta f_T \approx 30$ kHz, one yields the measured value $\delta f_M = V/2D_M \approx 36.69$ kHz, which leads to the experimentally obtained spectral resolution $\delta\lambda_M = \lambda \delta f_M / f_2 \approx 0.07821$ Å. at $\lambda = 405$ nm. Then, $\Delta\lambda_M = \Delta f_M \lambda/f_2 \approx 7.503$ Å (instead of the theoretical value $\Delta\lambda_T \approx 7.35$ Å because of damping the transducer). Thus the experiment gives a number of resolvable spots is $N_M = \Delta f_M / \delta f_M = \Delta\lambda_M / \delta\lambda_M \approx 96$ spots.

Generally, the LiNbO$_3$ crystal has rather high refractive indices, for example, the value about $n_O = 2.432$ and $n_E = 2.422$ at $\lambda = 405$ nm were used during the experiments. This is why one can expect significant optical attenuation inside the crystal and remarkable reflections from the facets of that AO cell. Undoubtedly, to minimize potential optical losses the facets of AO cell ought to have anti-reflection coating. Nevertheless, we had performed our proof-of-principle experiments with the AO cell that had not been coated. Therefore, the relative efficiency of light scattering into the second order had been first experimentally estimated and then measured at the output facet of the AO cell. In so doing, the light intensity detected at the output facet, transmitted through the cell in the absence of an external UHF electronic excitation, had been counted as the unity. The light intensity scattered into the second order in the presence of that electronic signal and measured at the output facet had been considered as the usable optical signal caused by UHF electronic signal. The ratio of this usable optical signal to the initially transmitted light intensity (both are measured at the output facet of that AO cell), one can consider as the relative efficiency of light scattering. Thus the relative efficiency, determined as it has been described above, had been measured at the optimal acoustic frequency $f_2 \approx 1.9$ GHz at $\lambda = 405$, 532, and 633 nm as well. The maximum relative efficiency at $\lambda = 405$ nm had been experimentally estimated by the value ∼ 0.81. In Table **3**, the comparison of theoretical and experimental results is presented. One can see that some experimentally obtained data, namely, the frequency and spectral bandwidths as well as the numbers of resolvable spots exhibit general tendency to be very close to the above-calculated theoretical values. This tendency takes place despite the presence of natural imperfectness peculiar to all the optical components in our experimental set-up. Similar result can be attributed to the use of damping the piezoelectric transducer in the developed AO cell.
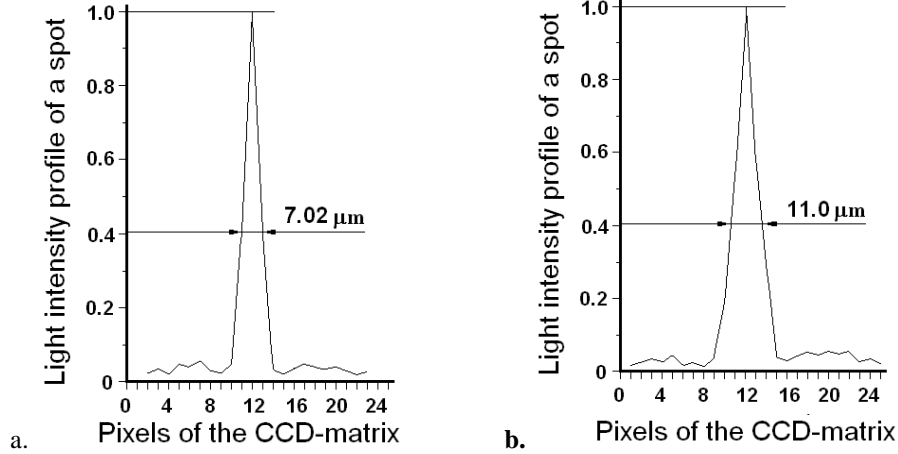
Fig. 6 Light intensity profiles of an individual resolvable spot for the LiNbO$_3$-based AO cell: (a) λ = 405 nm and (b) λ = 633 nm.

The experimental results obtained with the reduce-aperture, i.e. 6-cm lithium niobate AO cell (the spectral resolution $\delta\lambda_M \approx 0.0782$ Å at λ = 405 nm and the resolving power R_M = 51,790) have a gain compared with the most advanced to our knowledge, AO spectrometers for space or airborne operations of the twenty-first century [22,23], even with the recently obtained ones [12]. However, the achieved spectral bandwidth $\Delta\lambda_M \approx 7.503$ Å and $N_M \approx 96$ spots cannot be considered as an acceptable data by itself. Nevertheless, within the above-developed 2-step synthesis approach, i.e. together with prism cross disperser, one arrives at definitely high results, which include all the visible range as spectral bandwidth $\Delta\lambda$ with the total number of resolvable spots about ~10,000 or more. By this it means that our new experimental result for the above-described two-step spectrometer (with the increased operation frequency and higher acceptable acoustic losses per optical aperture) can be considered as the best one can mention at the moment.

Table 3. Comparison of theoretical and experimental data; f_2 = 1.9 GHz, $\delta f_T \approx 30$ kHz, and $\delta f_M \approx 36.69$ kHz.

λ, nm	$\kappa\, d_T$, μm	Δf_T, MHz	Δf_M, MHz	d_M, μm	$\Delta\lambda_T$, Å	$\Delta\lambda_M$, Å	$\delta\lambda_T$, Å	$\delta\lambda_M$, Å	N_T	N_M
405	5.967	3.43	3.52	7.02	7.35	7.503	0.0643	0.0782	114	96
532	7.612	2.49	2.61	8.96	7.03	7.308	0.0845	0.1028	83	71
633	9.326	2.06	2.16	10.97	6.91	7.196	0.1005	0.1223	68	59

7. DISCUSSION AND CONCLUSION

We have proposed a new approach to the development of optical spectrometer with a wide-aperture AO dynamic grating for the Guillermo Haro astrophysical observatory (Mexico). Initially, a few crystalline materials had been characterized to select $LiNbO_3$ as the most acceptable option. Then, the two-phonon light scattering in this crystal had been characterized to reveal preliminary the expected benefits from possible development. The problems of characterization were not trivial due to $LiNbO_3$ is the trigonal crystal in contrast with the tetragonal ones considered before. As a result, the progressed development includes two novelties. One of them consists in applying recently identified and studied AO nonlinearity specific to the two-phonon light scattering in crystals with linear acoustic losses. This kind of light scattering gives us ultimately an opportunity to create the specific AO cell providing extremely high spectral resolution together with the nonlinear apodization even within the standard scheme of AO spectrum analyzer. The second novelty implies exploiting the cross-disperser technique together with AO processing of optical signals. Similar pioneer synthesis allows us to operate over all the visible range and even more in parallel regime with maximal spectral resolution. In so doing, our investigations include two closely connected parts. At first, the total theoretical analysis and the needed estimations have been produced for a 9-cm $LiNbO_3$ AO cell, whose size is directly correlated with the observation window of optical spectrometer in that observatory. After that, we develop a concept for combining the cross-disperser technique with precise AO spectrum analysis optical signals. As a result, the scheme under proposal would be able to shape at its output a 2D-spectral distribution characterizing simultaneously, for example at $\lambda = 405$ nm, more than 57,500 resolvable spots in the visible range with spectral resolution 0.0523 Å with the resolving power $R \approx 77,140$ and efficiency of operation $\sim 100\%$. Nevertheless, the experiment's detector should follow the sampling theorem [21], so the requirement is set as a CCD matrix with a minimum of 472×488 pixels. Then, it should be noted that the estimations will be significantly changed at $\lambda = 633$ nm, so that one will have $N \times M = 126 \times 156 = 19,600$ spots. Consequently, an acceptable number of pixels within the CCD photo-detector can be taken the same as more as a spot's size at this light wavelength will be even larger.

Finally, we demonstrate numerically and confirm during proof-of-principle experiments only for AO part of the joint scheme that the principle possibility exists to realize similar combined spectrometer using the available 6-cm $LiNbO_3$ crystalline AO cell. Unfortunately, this crystal is about 1000 times less effective than calomel, exploited before, so that we were forced the carry out these illustrative experiments in the electronically pulsed regime. The pulsed operation of AO cell can be exploited practically during astrophysical observations with the regime of accumulation. In this case, the pulsed operation of AO cell will only decreases the efficiency in the whole system and increases the time of integration. Nevertheless, the CW operation might be suitable for $LiNbO_3$ cell as well in the case of very effective heat removal within the integrated solid state cooling system that can be realized due to a sufficiently high heat resistance of $LiNbO_3$ crystal.

Moreover, the available crystal was not doped by Mg that reduced its efficiency in blue part of the spectrum. These performances obtained from the experiment with undoped $LiNbO_3$ can be re-estimated for the optimal 4% Mg doped $LiNbO_3$ crystal [10]. In so doing, one

could formulate the refined requirements to the needed CCD matrix. However, we have used very low optical power density (as it is expected within astrophysical applications), as more as in this case the data obtained from the available 6-cm $LiNbO_3$ crystalline AO cell lie mainly in the correspondence with the performed analytical and numerical estimations. The achieved spectral resolution $\delta\lambda_M \approx 0.0782$ Å at $\lambda = 405$ nm and the resolving power 51,790 are the best to our knowledge at the moment for AO spectrometers dedicated to space or airborne operations [6,7,22,23]. Finally, one can say that these data represent a further progress in designing an AO innovative technique in an advanced optical spectrum analysis with the significantly enhanced spectral resolution.

ACKNOWLEDGEMENTS

REFERENCES

[1]   S. E. Harris and R. W. Wallace, "Acousto-Optic Tunable Filter," J. Opt. Soc. Am. 59 (6), 744-747 (1969).

[2]   I.C. Chang, "Tunable Acousto-Optic Filters: An Overview", Proc. SPIE 0090, Acousto-Optics: 12-22 (1976).

[3]   A.Korpel. *Acousto-Optics*, 2nd Ed., N.-Y., (Marcel Dekker, 1997).

[4]   V. I. Balakshy, V. N. Parygin, and L. I. Chirkov. *Physical Principles of Acousto-Optics*, Radio I Svyaz, Moscow, (1985).

[5]   J. Xu and R. Stroud, *Acousto-Optic Devices: Principles, Design and Applications* (Wiley, 1992).

[6]   J. L. Bertaux et al. In European Space Agency; SP-1240 "Mars Express: A European mission to the red planet." Edited by Wilson A (ESA Publications Division) (2004).

[7]   J. L. Bertaux et al., "SPICAV on Venus Express: Three spectrometers to study the global structure and composition of the Venus atmosphere", Planetary and Space Science 55 (12) 1673-1700 (2007).

[8]   A. S. Shcherbakov, A. O. Arellanes, V. Chavushyan, "Optical spectrometer with acousto-optical dynamic grating for Guillermo Haro Astrophysical Observatory", International Journal of Astronomy and Astrophysics, Vol. 3, 376-384, (2013).

[9]   A. S. Shcherbakov, A. O. Arellanes, S. A. Nemov, "Transmission function collinear acousto-optical interaction occurred by acoustic waves of finite amplitude", J. Opt. Soc. Am. B, vol. 30, No. 12, 3174-3183, (2013).

[10]   A. S. Shcherbakov, A. O. Arellanes, and E. Bertone, "Advanced collinear LiNbO3 acousto-optical filter for astrophysical spectroscopy in the near ultraviolet: exploring the high spectral resolution", J. Astron. Telesc. Instrum. Syst. 1(4), 045002 (2015).

[11]   A. S. Shcherbakov and A. O. Arellanes, "Advanced regime of the noncollinear two-phonon acousto-optical interaction governed by elastic waves of finite amplitude and optical spectrum analysis", J. Opt. Soc. Am. B Vol. 32, No. 9, 1930-1940 (2015).

[12]   A. S. Shcherbakov and A. O. Arellanes, "Calomel-made crystalline acousto-optical cell designed for an advanced regime of noncollinear two-phonon light scattering", Opt. Eng. 55(3), 037107 (2016).

[13]   S. S. Vogt, "HIRES - a High Resolution Echelle Spectrometer for the Keck Ten-Meter Telescope", Symposium on Astronomical Telescopes & Instrumentation for the 21st Century, International Society for Optics and Photonics, pp. 362-375 (1994).

[14]   A. P. Goutzoulis and D. R. Pape, *Design and fabrication of acousto-optic devices* (Marcel Dekker, 1994).

[15]   N. Uchida and N. Niizeki, "Acoustooptic deflection materials and techniques", Proc. IEEE, Vol. 61, No. 8, 1073-1092, (1973).

[16]   M. P. Shaskolskaya, Acoustic Crystals, Moscow, (Nauka, 1982).

[17]   I. C. Chang, "Acousto-Optic Devices and Applications" in Handbook of Optics Vol. II Devices, Measurements, and Properties, M. Bass Ed., (McGraw-Hill, 1995).

[18]   L. W. J. Kent, "3 GHz bandwidth rutile Bragg cell", Proc. of SPIE, vol. 7100, 710027-1 (2008).

[19]   W. L. Wolfe, *Introduction to imaging spectrometers*, SPIE (Washington, 1997).

[20]   Thorlabs Catalog, Optical Substrates (2016).

[21]   A. Papoulis, *Systems and transforms with applications in optics* (Krieger Pub Co, 1981).

[22]   F.P. Helmich, "Herschel HIFI—The Heterodyne Instrument for the Far-Infrared", European Astronomical Society Publications Series, 52, 15-20 (2011).

[23]   S. Heyminck, U. U. Graf, R. Güsten, J. Stutzki, H. W. Hübers, and P. Hartogh, "GREAT: the SOFIA high-frequency heterodyne instrument", A&A Vol. 542 L1 (2012).